Inorganic Chemistry

pubs.acs.org/IC
Article

Modulation of the Dynamics of a Two-Dimensional Interweaving Metal−Organic Framework through Induced Hydrogen Bonding

Pilar Fernández-Seriñán, Kornel Roztocki, Vahid Safarifard, Vincent Guillerm, Sabina Rodríguez-Hermida, Judith Juanhuix, Inhar Imaz,* Ali Morsali,* and Daniel Maspoch*

Cite This: *Inorg. Chem.* 2024, 63, 5552−5558
Read Online

ACCESS | Metrics & More | Article Recommendations | Supporting Information

ABSTRACT: Inducing, understanding, and controlling the flexibility in metal−organic frameworks (MOFs) are of utmost interest due to the potential applications of dynamic materials in gas-related technologies. Herein, we report the synthesis of two isostructural two-dimensional (2D) interweaving zinc(II) MOFs, TMU-27 [Zn(bpipa)(bdc)] and TMU-27-NH_2 [Zn(bpipa)(NH_2-bdc)], based on *N*,*N*′-bis-4-pyridyl-isophthalamide (bpipa) and 1,4-benzenedicarboxylate (bdc) or 2-amino-1,4-benzenedicarboxylate (NH_2-bdc), respectively. These frameworks differ only by the substitution at the meta-position of their respective bdc groups: an H atom in TMU-27 vs an NH_2 group in TMU-27-NH_2. This difference strongly influences their respective responses to external stimuli, since we observed that the structure of TMU-27 changed due to desolvation and adsorption, whereas TMU-27-NH_2 remained rigid. Using single-crystal X-ray diffraction and CO_2-sorption measurements, we discovered that upon CO_2 sorption, TMU-27 undergoes a transition from a closed-pore phase to an open-pore phase. In contrast, we attributed the rigidification in TMU-27-NH_2 to intermolecular hydrogen bonding between interweaving layers, namely, between the H atoms from the bdc-amino groups and the O atoms from the bpipa-amide groups within these layers. Additionally, by using scanning electron microscopy to monitor the CO_2 adsorption and desorption in TMU-27, we were able to establish a correlation between the crystal size of this MOF and its transformation pressure.

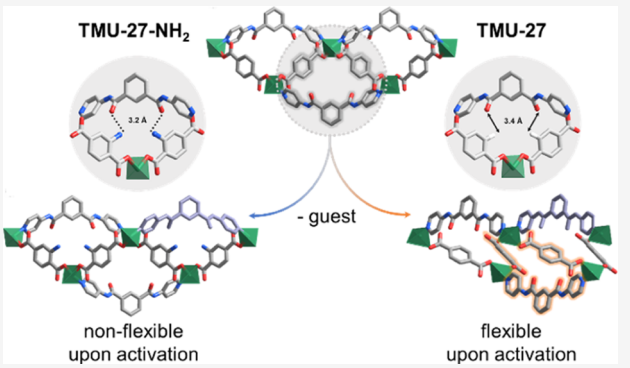

INTRODUCTION

Metal−organic frameworks (MOFs) are porous materials made by combining metal ions or clusters with organic linkers and can be designed for practical applications.[1] There are countless available building blocks for MOFs, the nearly infinite combinations of which can yield novel materials with unprecedented structural and functional properties. The systematic study of structure−function relationships in MOFs has afforded presynthesis design strategies such as reticular synthesis[1] or crystal engineering.[2]

Among the many ways to classify MOFs, one is by their structural flexibility, with relatively rigid MOFs representing a large group and flexible or dynamic-porous MOFs[3] comprising a much smaller group.[4,5] Here, flexibility refers to the dynamic responses of MOF structures to stimuli such as changes in temperature,[6−8] pressure,[9,10] light,[11] and electrical fields[12] or, most commonly, during host−guest interactions.[13] Interestingly, MOFs respond to stimuli through diverse mechanical mechanisms such as breathing,[14] swelling,[15] linker rotation, or subnetwork displacement,[3,16] all of which involve deformation of their pores and appear, on isotherms, as peculiar singularities.[17] These mechanisms are dictated by three main factors: (i) the nature of the inorganic molecular building blocks;[13,18] (ii) the rotational freedom of the organic linker;[19] and (iii) the topology of the framework.[13] Moreover, features stemming from the supramolecular nature of a MOF structure, such as intermolecular interactions within the structure itself or between the structure and the guest, must also be considered.[13,20,21]

Metal−organic frameworks typically boast excellent surface areas, tunable pore sizes, and physicochemical robustness, making them of great interest for practical applications.[22−28] Importantly, adding or increasing the flexibility in MOFs can enhance their performance in various fields. For example, in catalysis,[29] it allows for the formation of stimuli switching catalysts; in molecular sensing, it enables specific host−guest interactions;[30] and in drug delivery, it improves control over conditional release.[31] Additionally, flexibility can enable separation of water isotopologues, namely, via controlled

Received: December 20, 2023
Revised: February 22, 2024
Accepted: February 27, 2024
Published: March 14, 2024

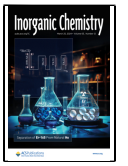

https://doi.org/10.1021/acs.inorgchem.3c04522
Inorg. Chem. 2024, 63, 5552−5558

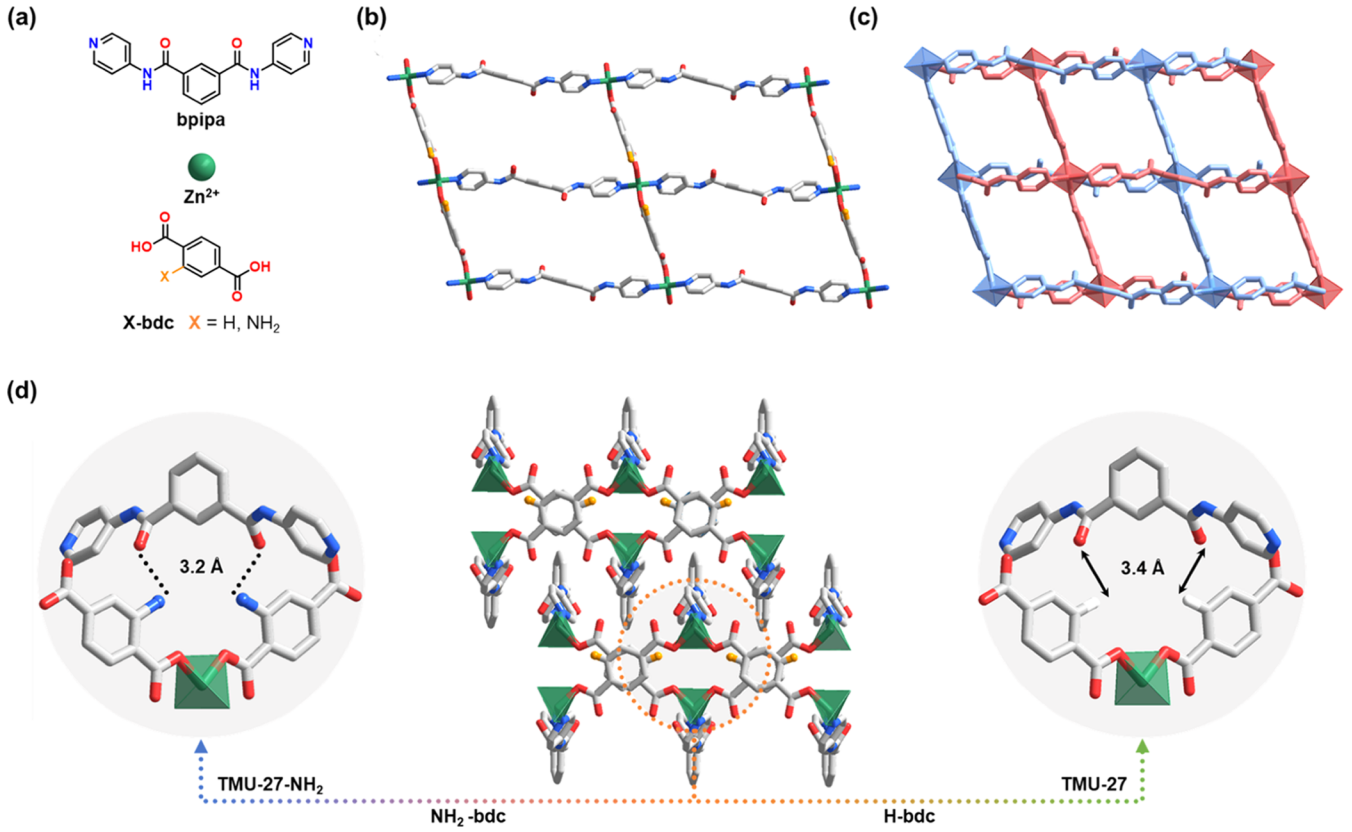

Figure 1. Synthesis and structural analysis of TMU-27 and TMU-27-NH_2. (a) Representation of the respective molecular building units (TMU-27: X = H; TMU-27-NH_2: X = NH_2). (b) Representation of a single layer. (c) Interweaving layers, in which each layer is represented with a different color. (d) Interdigitation of the interweaving layers (center). Highlight of the hydrogen bonding between interdigitated layers in TMU-27-NH_2 (left) in stark contrast to the lack of such bonding in TMU-27 (right).

diffusion through the dynamic aperture of pores,[32] enhanced proton conductivity,[33] and improved gas storage[17,34,35] or separation[36] through expanded storage capacities and potential selectivity.

While researchers have identified flexible MOFs and studied their mechanisms of transformation, relatively little progress has been made on inducing and controlling flexibility in MOFs or similar porous materials. A few recent examples have revealed that single-atom substitutions in organic linkers can alter phase transition mechanisms (e.g., from a stepwise transformation into a continuous one)[37,38] or lead to changes in the isotherm type.[37−39] Furthermore, there are reports that crystal size may influence the adsorption properties of flexible MOFs,[35,40] which in turn might relate to shape-memory effects,[41] negative gas adsorption,[42] or even rigidification.[40] However, before a priori design of flexible MOFs can be functional, a better fundamental understanding of the features that trigger and control their dynamic behavior is needed.[43,44]

Here, we report the design and synthesis of a novel flexible two-dimensional (2D) interweaving MOF with formula [Zn(bpipa)(bdc)]·2DMF (hereafter called TMU-27; bpipa = *N*,*N*′-bis-4-pyridyl-isophthalamide and bdc^{2-} = terephthalate) as well as of its more rigid counterpart, [Zn(bpipa)(NH_2-bdc)]·2DMF (hereafter called TMU-27-NH_2; NH_2-bdc^{2-} = amino terephthalate). Note that these MOFs differ only by the substitution at the meta-position of their respective bdc groups: an H atom in TMU-27 vs an NH_2 group in TMU-27-NH_2. While the introduction of aromatic amines into MOFs usually has only a negligible to moderate impact on its sorption properties,[45,46] TMU-27-NH_2 is a rare example in which the impact is instead quite dramatic, as we report here. Indeed, by comparing the two isoreticular MOFs, in both the presence and absence of guest molecules in their pores, through a detailed structural analysis by single-crystal and powder X-ray diffraction (SC- and PXRD) and CO_2-sorption measurements (taken at 203 K), we observed that TMU-27 is flexible upon CO_2 sorption/desorption and that this flexibility is blocked in TMU-27-NH_2 by the introduction of a single functional amino group in the organic linker. Additionally, through monitoring of repetitive CO_2 adsorption and desorption in TMU-27, using scanning electron microscopy (SEM), we were able to establish a correlation between its transformation pressure and its crystal size.

EXPERIMENTAL SECTION

Synthesis of bpipa. Isophthaloyl chloride (1.015 g, 5 mmol) was slowly added to a solution of 4-aminopyridine (1.882 g, 20 mmol) in 25 mL of dry THF. The resulting mixture was refluxed for 24 h, ultimately affording a white product. The solid was filtered off and poured into an aqueous solution of saturated Na_2CO_3, and the resulting mixture was stirred. The product was filtered off, washed with dichloromethane, methanol, and water, and then dried at 100 °C for 3 h to afford a white solid (yield: 91%).

Synthesis of TMU-27-NH_2. A mixture of $Zn(NO_3)_2·6H_2O$ (0.027 g, 0.09 mmol), NH_2-bdc (0.016 g, 0.09 mmol), bpipa (0.029 g, 0.09 mmol), and DMF (9 mL) was sonicated until all of the solids were uniformly dispersed and was then heated at 120 °C for 24 h. This afforded brown crystals as a pure phase, which were washed with DMF. Activation at 160 °C for 3 h led to solvent removal from the pores (yield: 64%). FT-IR (cm^{-1}): 1670 (vs), 1564 (vs), 1509 (vs),

https://doi.org/10.1021/acs.inorgchem.3c04522
Inorg. Chem. 2024, 63, 5552−5558

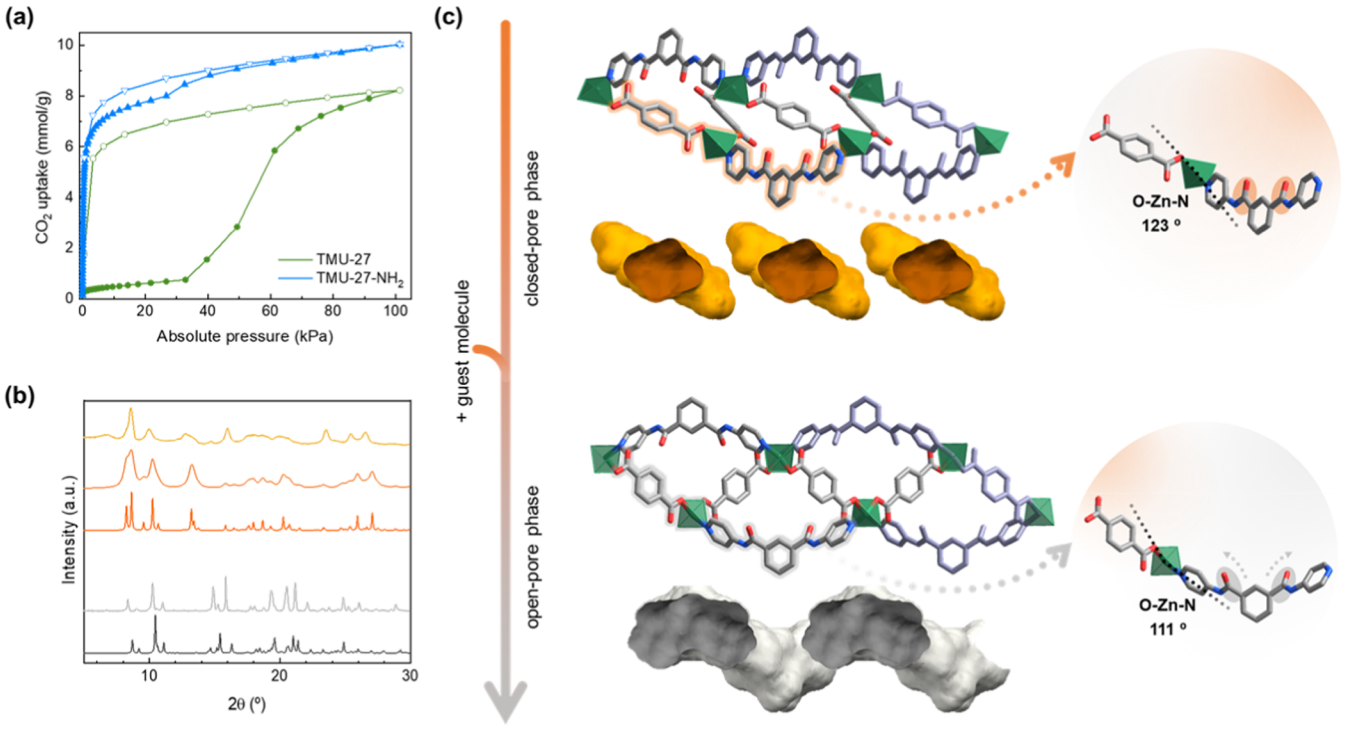

Figure 2. (a) Isotherms of the CO_2 sorption at 203 K for TMU-27 (green) and TMU-27-NH_2 (blue). Key: filled circles or triangles = adsorption branch; hollow circles or triangles = desorption branch. (b) Simulated (from SC-XRD) and experimental PXRD patterns for the closed-pore (CP) phase (top; dark orange = simulated; light orange = experimental, measured at 160 °C) and the open-pore (OP) phase (bottom; black = simulated; gray = experimental, measured at 160 °C) of TMU-27. To include disorder created in response to the removal of guest molecules in the CP phase, the FWHM of the simulated PXRD pattern (top, middle) was increased to 0.8·2θ, matching the experimental pattern. (c) Representation of the evolution from the CP phase to the OP phase in TMU-27.

1433 (vs), 1330 (vs), 1303 (s), 1250 (s), 1207 (s), 1087 (m), 1064 (m), 1031 (m), 837 (vs), 770 (s), 597 (s), 526 (s). Elemental analysis calcd (%) for TMU-27-NH_2: C 54.21, H 4.69, N 13.83; found: C 50.24, H 4.44, N 12.60.

Synthesis of TMU-27. A mixture of $Zn(NO_3)_2{\cdot}6H_2O$ (0.036 g, 0.2 mmol), bdc (0.020 g, 0.2 mmol), bpipa (0.038 g, 0.2 mmol), water (1.2 mL), acetic acid (160 μL), and DMF (10.8 mL) was sonicated until all of the solids were uniformly dispersed and was then heated at 85 °C for 24 h. This afforded white needle-shaped crystals, which were obtained as a pure phase and then washed with DMF. Activation at 160 °C under vacuum for 6 h led to solvent removal from the pores, resulting in the formation of the CP phase (yield: 71%). FT-IR (cm^{-1}): 1673 (s), 1593 (vs), 1503 (vs), 1434 (m), 1385 (vs), 1332 (s), 1304 (s), 1233 (m), 1207 (s), 1032 (m), 837 (s), 748 (s), 597 (m), 537 (m). Elemental analysis calcd (%) for TMU-27: C 55.38, H 4.65, N 12.11; found: C 54.6, H 4.53, N 11.6

Materials and Characterization. All commercially available reagents were used without further purification. Powder X-ray diffraction (PXRD) measurements were taken on an X'pert Pro MPD-Malvern PANalytical diffractometer with monochromatic Cu-Kα radiation (λCu = 1.5406 Å). Nonambient PXRD measurements were performed in a TTK600 Low-Temperature Chamber from Anton Paar, which was mounted inside the diffractometer, allowing for the use of a temperature range from −20 to 600 °C and in air/vacuum conditions. Fourier transform infrared (FT-IR) spectra were recorded on a Bruker Tensor 27FTIR spectrometer equipped with a Golden Gate, diamond, attenuated total reflection (ATR) cell in absorption mode at room temperature. Thermogravimetric analyses (TGA) were run in a PerkinElmer Pyris 1 under a N_2 atmosphere and a heating rate of 10 °C/min. Scanning electron microscopy (SEM) was performed using a Quanta 650FEG SEM and a Magellan 400L XHR SEM. CO_2- and N_2-sorption isotherms were collected at 203 and 77 K, respectively, using an ASAP 2020 HD (Micromeritics). Temperature was controlled by using a liquid nitrogen bath (77 K) or a Lauda Proline RP 890 chiller (203−298 K). Total pore volumes (V_t) were calculated at P/P_0 = 0.95 (N_2).

RESULTS AND DISCUSSION

We began with the synthesis of TMU-27. To this end, a mixture of $Zn(NO_3)_2{\cdot}6H_2O$, bpipa, and H_2bdc in water, acetic acid, and DMF was heated at 85 °C for 1 day to afford white, needle-shaped crystals of TMU-27 (Figure 1a). The SC-XRD analysis of TMU-27 revealed that it crystallizes in a monoclinic lattice, with the $P21/c$ space group (Table S1 in the SI). In this structure, each zinc ion is tetracoordinated in a slightly distorted tetrahedral geometry, bound to two N atoms on two bpipa linkers (Zn−N bond distance: 2.005(3) Å) and to two O atoms in monodentate carboxylate groups on two bdc linkers (Zn−O bond distance: 1.956(4) Å) (Figure S2a), leading to an overall 4-connected bidimensional network exhibiting an underlying **sql** topology (Figures 1b and S2c,d in the SI). Due to the alternating upward−downward orientation of the V-shaped bpipa ligand, the layers are interwoven (Figure 1c), leading to an overall stacking/interdigitating of interwoven 2D layers due to short contacts between the secondary amines from the bpipa ligand and the O atom from the bdc/NH_2-bdc that does not participate in the metal−ligand coordinative bond. Zn equivalent positions are separated by a distance of 11.999(18) Å (Figure 1d), and this stacking results in the formation of one-dimensional (1D) open channels with a pore window size of 3.9 Å and a maximal pore diameter of 5.5 Å (Figures 2c and S3 in the SI).

Next, we synthesized TMU-27-NH_2. Similarly to the previous reaction, a mixture of $Zn(NO_3)_2{\cdot}6H_2O$, bpipa, and NH_2-bdc in DMF was heated at 120 °C for 1 day to afford

https://doi.org/10.1021/acs.inorgchem.3c04522
Inorg. Chem. 2024, 63, 5552−5558

rhombohedron-shaped brown crystals of TMU-27-NH_2. Detailed crystallographic analysis revealed that it crystallizes in a monoclinic lattice with the $C2/c$ space group and **sql** topology, similarly to TMU-27. Thus, TMU-27-NH_2 is isostructural to TMU-27; however, it shows additional intermolecular hydrogen-bonding interactions [NH···O between the NH group from the NH_2-bdc and the amide O atoms of bpipa; bond distance: 3.1 Å (Figure 1d)] between each pair of interwoven layers. Equivalent Zn positions in 2D-stacked layers are separated by a distance of 11.864(16) Å. The simulated PXRD patterns for TMU-27-NH_2 and TMU-27 match with the corresponding patterns for the as-synthesized materials (Figures 2b and S4 in the SI). Also, their respective elemental analyses coincide with the expected formulas, indicating that the crystal structures are representative of the bulk materials.

Next, we evaluated the thermal stability of TMU-27 and TMU-27-NH_2. Subsequent thermogravimetric analysis (TGA) revealed initial weight-loss values of 19.2% for TMU-27 and 19.8% for TMU-27-NH_2, which we attributed to the loss of the guest solvent molecules (expected values: 21.0% for TMU-27, [Zn(bpipa)(bdc)]·2DMF, and 20.6% for TMU-27-NH_2, [Zn(bpipa)(NH_2-bdc)]·2DMF). Both frameworks began to decompose between 300 and 350 °C, suggesting high thermal stability for each (Figure S6 in the SI).

We then proceeded to perform CO_2-sorption experiments on TMU-27 and TMU-27-NH_2. Considering the thermal stabilities of these two MOFs, we activated them at 160 °C for either 6 h (TMU-27) or 3 h (TMU-27-NH_2), prior to the CO_2 sorption, which we measured at 203 K (Figure 2a). The desolvated phase of each MOF exhibited distinct CO_2-driven adsorption properties. For TMU-27, the isotherm presents a sharp step at 32 kPa, corresponding to a type F-III adsorption isotherm (Figure 2a).[17] Such distinctive isotherms are characteristic of flexible materials and exhibit a phase transformation from a closed-pore (CP) phase, which is formed upon desolvation/activation of the as-synthesized TMU-27 (Figure 2b), to an open-pore (OP) phase, upon adsorption of guest species (Figures 2c and S8 in the SI). Importantly, we confirmed the presence of such a CP phase in the desolvated TMU-27 by SC-XRD analysis. This phase has a triclinic lattice with the $P\bar{1}$ space group. In comparison to the OP phase, the CP phase results from changes within the geometry of the bpipa ligand, which becomes planar, and a change in the bdc−Zn−bpipa angle, from 111° (OP) to 123° (CP), as shown in Figure 2c. These changes in the framework lead to disconnection of the 1D channels observed in the OP phase, resulting in the formation of a compartmentalized framework of discrete cavities (maximal pore diameter: 4.5 Å) and a simultaneous reduction of 23.2% in the unit-cell volume from the OP to the CP phases (Table S2 in the SI).

We observed that during the initial stage of adsorption, the CO_2 molecules diffused into the discrete cavities of the CP phase, resulting in an uptake of 0.8 mmol/g, which corresponds to the formula [Zn(bpipa)(bdc)]·0.5CO_2 (Figure 2a). Next, the internal pressure increased as the pores continued to fill, which eventually led to the migration of the CO_2 molecules between cavities. Once the pressure surpassed 32 kPa, this induced structural changes within the framework, resulting in further adsorption of CO_2. As previously demonstrated,[47] this process may occur due to the elasticity of the framework, which in this case would be induced by the rotation of the bdc benzene ring, which would block access to the separate cavities. The maximal CO_2 uptake that we observed for TMU-27 was 8.1 mmol/g at 101 kPa, which corresponds to the formula [Zn(bpipa)(bdc)]·3CO_2. According to Gurvich's rule, CO_2 in the pores of the OP phase would have occupied a volume of 0.33 cm^3/g. This value slightly exceeds the maximal theoretical pore volume of 0.31 cm^3/g, as calculated based on the assumption that the probe radius corresponds to the size of one CO_2 molecule.

Interestingly, the initial stage of the isotherm of TMU-27-NH_2 follows a pattern typical of microporous rigid materials that exhibit a type I adsorption isotherm.[48] In this case, CO_2 molecules (kinetic diameter: 3.30 Å) efficiently diffused into the pores (window size: 4.2 Å), reaching a maximum uptake of 10.0 mmol/g at a pressure of 101 kPa. We observed that during desorption there was a slight hysteresis, which indicated a different desorption mechanism to that of adsorption. Structural analysis of the desolvated TMU-27-NH_2 by SC-XRD proved the structure to be robust upon desolvation. Indeed, comparison of the pristine and desolvated TMU-27-NH_2 revealed only a minor contraction in the distance between the NH_2 group from the functionalized bdc linker and the O atom from the bpipa ligand: 3.2 Å in the pristine framework vs 3.1 Å in the desolvated form. These minor changes observed in the desolvated TMU-27-NH_2 concluded in a minor reduction of 2% in the cell volume (Table S1 and Figure S7 in the SI). Thus, we reasoned that the hydrogen-bonding network resulting from the presence of NH_2 from the functionalized bdc linker maintains the overall structure of the framework, effectively rigidifying it upon desolvation.

To further investigate the two isostructural MOFs, we measured their adsorption of N_2 at 77K (Figure S9 in the SI). The CP phase of TMU-27 was almost nonporous for N_2, showing that, in contrast to CO_2, N_2 cannot diffuse into the cavities and open the pores. Contrariwise, TMU-27-NH_2 is porous to N_2 and adsorbs 7.4 mmol/g at 95 kPa, presenting a Brunauer−Emmett−Teller (BET) area of 689 m^2/g. These results further confirm the more rigid open structure of TMU-27-NH_2 upon activation. Moreover, the experimental pore volume of 0.25 cm^3/g for TMU-27-NH_2 matches well to the calculated volume of 0.26 cm^3/g. Again, we observed a different mechanism for desorption in TMU-27-NH_2 than for adsorption: it appeared as a slight hysteresis, which, together with the aforementioned changes in the cell volume of TMU-27-NH_2 during activation, indicated to us the existence of minor structural changes within the framework. However, we reasoned that these changes were substantially smaller than those in the case of TMU-27 due to the stabilizing effect of the hydrogen-bonding network (Table S1 and Figure S7 in the SI).

A critical and highly desirable feature of flexible MOFs is the reversibility of adsorption properties in cyclic experiments.[43] Thus, to further investigate the behavior of TMU-27, we measured its response to repeated cycles of CO_2 adsorption/desorption, which we monitored by SEM (Figure 3). Although the successive cycles exhibited comparable step-containment behavior, there was a remarkable shift in the gate-opening pressure from 32 kPa in the first isotherm down to 11 kPa in the second isotherm and, finally, up to 13 kPa in the third. Irrespective of the number of cycles, the total uptake of CO_2 by TMU-27 at 203 K remained constant: 8.1 mmol/g at 101 kPa, demonstrating that this MOF does indeed exhibit the reversibility of adsorption−desorption cycles under repeated stress. As revealed by SEM imaging, the adsorption/desorption stress led to milling of the samples (Figure 3b), which underwent a considerable reduction in crystal size from >100

https://doi.org/10.1021/acs.inorgchem.3c04522
Inorg. Chem. 2024, 63, 5552−5558

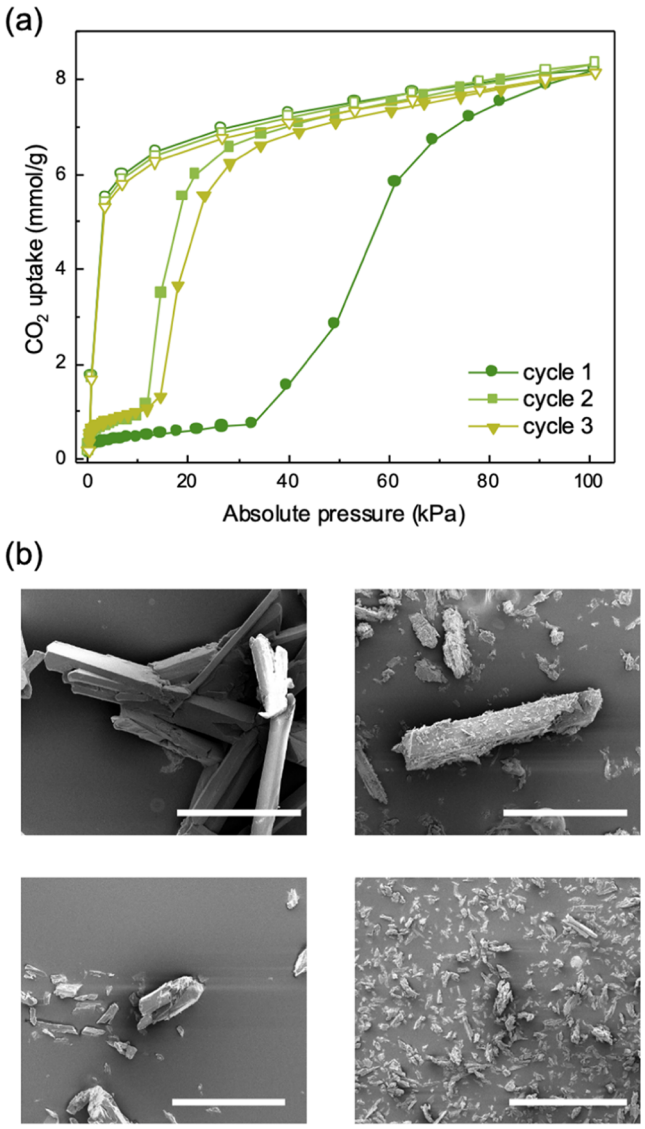

Figure 3. (a) Stability of the porosity of TMU-27 upon repeated cycles of CO_2 adsorption (solid symbols) and desorption (hollow symbols) at 203 K. (b) Scanning electron micrographs of the as-synthesized (top, left) and desolvated (top, right) TMU-27 as compared to TMU-27 after the first (bottom, left) and second (bottom, right) CO_2 adsorption/desorption cycle. Scale bars: 100 μm.

μm down to 55−65 μm (close to a 2-fold reduction) in the second isotherm and further down to 25−35 μm (close to a 5-fold reduction) in the third. This effect might lead to greater accessibility of CO_2 to the framework and to lower diffusion resistance due to a higher surface-area-to-volume ratio.[49] Nevertheless, considering that type F-III adsorption isotherms remained in subsequent sorption cycles, we deduced that this effect is insufficient to abrogate the flexibility of TMU-27.

CONCLUSIONS

Here, we have reported the synthesis of two 2D interweaving Zn-**sql**-MOFs, TMU-27 and TMU-27-NH_2, which differ in the substitution of their respective bdc linkers: an H atom in TMU-27 vs an NH_2 group in TMU-27-NH_2. While TMU-27 is nonporous to N_2 but highly flexible upon CO_2 sorption/desorption, TMU-27-NH_2 exhibits adsorption properties commonly found in rigid MOFs. In TMU-27-NH_2, the introduction of an amino group stabilizes the two-dimensional interweaving layers through hydrogen bonding. This hydrogen bonding prevents TMU-27-NH_2 to be flexible as it retains its original open-pore structure upon activation, making it porous to, for example, N_2 and CO_2. Flexibility in TMU-27 undergoes a change from an open-pore (OP) phase to a closed-pore (CP) phase upon activation. This flexibility is reactivated upon CO_2 adsorption, in which CO_2 can diffuse into the discrete cavities of the CP phase, resulting in the formation of a pore opening in the OP phase. TMU-27 returns to its CP phase upon CO_2 desorption. We elucidated these structural transformations of TMU-27 by SC- and PXRD studies and then through repeated CO_2-sorption measurements. When exposed to adsorption/desorption stress, TMU-27 undergoes a significant reduction in crystal size, resulting in a shift in the gate-opening pressure from 32 to ∼12 kPa; however, the total CO_2 uptake (8.1 mmol/g) remains constant. Therefore, the transition mechanism of adsorption does not change, but the energy of transformation decreases with a reduction in the crystal size. In conclusion, we have presented how the flexibility of a MOF can be modulated through induction of linker-dependent hydrogen bonding. Moreover, we are confident that our findings should inform future work on how the crystal size of stimuli-responsive porous materials influences their adsorption properties.

ASSOCIATED CONTENT

Supporting Information

The Supporting Information is available free of charge at https://pubs.acs.org/doi/10.1021/acs.inorgchem.3c04522.

Additional experimental details and materials and methods, including ^{1}H NMR of the ligand synthesis, X-ray crystallography and crystal data, FTIR, TGA, reversibility test, and N_2 adsorption (PDF)

Accession Codes

CCDC 2302105−2302108 contain the supplementary crystallographic data for this paper. These data can be obtained free of charge via www.ccdc.cam.ac.uk/data_request/cif or by emailing data_request@ccdc.cam.ac.uk or by contacting The Cambridge Crystallographic Data Centre, 12 Union Road, Cambridge CB2 1EZ, UK; fax: +44 1223 336033.

AUTHOR INFORMATION

Corresponding Authors

Inhar Imaz − *Catalan Institute of Nanoscience and Nanotechnology (ICN2), CSIC and The Barcelona Institute of Science and Technology, Bellaterra, Barcelona 08193, Spain; Chemistry Department of Autonomous, University of Barcelona (UAB), Bellaterra, Barcelona 08193, Spain;* orcid.org/0000-0002-0278-1141; Email: inhar.imaz@icn2.cat

Ali Morsali − *Department of Chemistry, Faculty of Sciences, Tarbiat Modares University, Tehran 14115-175, Iran;* Email: morsali_a@modares.ac.ir

Daniel Maspoch − *Catalan Institute of Nanoscience and Nanotechnology (ICN2), CSIC and The Barcelona Institute of Science and Technology, Bellaterra, Barcelona 08193, Spain; Chemistry Department of Autonomous, University of Barcelona (UAB), Bellaterra, Barcelona 08193, Spain; ICREA, Barcelona 08010, Spain;* orcid.org/0000-0003-1325-9161; Email: daniel.maspoch@icn2.cat

https://doi.org/10.1021/acs.inorgchem.3c04522
Inorg. Chem. 2024, 63, 5552−5558

Authors

Pilar Fernández-Seriñán − *Catalan Institute of Nanoscience and Nanotechnology (ICN2), CSIC and The Barcelona Institute of Science and Technology, Bellaterra, Barcelona 08193, Spain; Chemistry Department of Autonomous, University of Barcelona (UAB), Bellaterra, Barcelona 08193, Spain;* orcid.org/0000-0002-6456-7386

Kornel Roztocki − *Faculty of Chemistry, Adam Mickiewicz University, Poznań 61-614, Poland;* orcid.org/0000-0001-7102-9802

Vahid Safarifard − *Department of Chemistry, Iran University of Science and Technology, Tehran 16846-13114, Iran;* orcid.org/0000-0003-4876-8257

Vincent Guillerm − *Catalan Institute of Nanoscience and Nanotechnology (ICN2), CSIC and The Barcelona Institute of Science and Technology, Bellaterra, Barcelona 08193, Spain;* orcid.org/0000-0003-3460-223X

Sabina Rodríguez-Hermida − *Catalan Institute of Nanoscience and Nanotechnology (ICN2), CSIC and The Barcelona Institute of Science and Technology, Bellaterra, Barcelona 08193, Spain;* orcid.org/0000-0001-7671-9925

Judith Juanhuix − *ALBA Synchrotron, Cerdanyola del Vallès, Barcelona 08290, Spain;* orcid.org/0000-0003-3728-8215

Complete contact information is available at: https://pubs.acs.org/10.1021/acs.inorgchem.3c04522

Notes

The authors declare no competing financial interest.

■ ACKNOWLEDGMENTS

This work has received funding from the European Union's Horizon 2020 research and innovation programme under Grant Agreement No 101019003; the Grant ref PID2021-124804NB-I00 funded by MCIN/AEI/10.13039/501100011033/ and by "ERDF A way of making Europe"; and the Catalan AGAUR (project 2021 SGR 00458). It was also funded by the CERCA Programme/Generalitat de Catalunya. ICN2 is supported by the Severo Ochoa Centres of Excellence programme, Grant CEX2021-001214-S, funded by MCIN/AEI/10.13039.501100011033. It was also supported by Tarbiat Modares University. K.R. gratefully acknowledges the support of the National Science Centre (NCN) of Poland (Grant No. 2020/36/C/ST4/00534).

■ REFERENCES

(1) Yaghi, O. M.; O'Keeffe, M.; Ockwig, N. W.; Chae, H. K.; Eddaoudi, M.; Kim, J. Reticular synthesis and the design of new materials. *Nature* **2003**, *423* (6941), 705−714.

(2) Allendorf, M. D.; Stavila, V. Crystal engineering, structure−function relationships, and the future of metal−organic frameworks. *CrystEngComm* **2015**, *17* (2), 229−246.

(3) Schneemann, A.; Bon, V.; Schwedler, I.; Senkovska, I.; Kaskel, S.; Fischer, R. A. Flexible metal−organic frameworks. *Chem. Soc. Rev.* **2014**, *43* (16), 6062−6096.

(4) Khan, M. Y.; Shahid, M. A contemporary report on explications of flexible metal-organic frameworks with regards to structural simulation, dynamics and material applications. *Polyhedron* **2022**, *225*, No. 116041.

(5) Li, X.; Sensharma, D.; Koupepidou, K.; Kong, X.-J.; Zaworotko, M. J. The Effect of Pendent Groups upon Flexibility in Coordination Networks with Square Lattice Topology. *ACS Mater. Lett.* **2023**, *5*, 2567−2575.

(6) Boutin, A.; Bousquet, D.; Ortiz, A. U.; Coudert, F.-X.; Fuchs, A. H.; Ballandras, A.; Weber, G.; Bezverkhyy, I.; Bellat, J.-P.; Ortiz, G.; Chaplais, G.; Paillaud, J.-L.; Marichal, C.; Nouali, H.; Patarin, J. Temperature-Induced Structural Transitions in the Gallium-Based MIL-53 Metal−Organic Framework. *J. Phys. Chem. C* **2013**, *117* (16), 8180−8188.

(7) Formalik, F.; Neimark, A. V.; Rogacka, J.; Firlej, L.; Kuchta, B. Pore opening and breathing transitions in metal-organic frameworks: Coupling adsorption and deformation. *J. Colloid Interface Sci.* **2020**, *578*, 77−88.

(8) Liu, Y.; Her, J.-H.; Dailly, A.; Ramirez-Cuesta, A. J.; Neumann, D. A.; Brown, C. M. Reversible Structural Transition in MIL-53 with Large Temperature Hysteresis. *J. Am. Chem. Soc.* **2008**, *130* (35), 11813−11818.

(9) Beurroies, I.; Boulhout, M.; Llewellyn, P. L.; Kuchta, B.; Férey, G.; Serre, C.; Denoyel, R. Using Pressure to Provoke the Structural Transition of Metal−Organic Frameworks. *Angew. Chem., Int. Ed.* **2010**, *49* (41), 7526−7529.

(10) Wieme, J.; Rogge, S. M. J.; Yot, P. G.; Vanduyfhuys, L.; Lee, S.-K.; Chang, J.-S.; Waroquier, M.; Maurin, G.; Van Speybroeck, V. Pillared-layered metal−organic frameworks for mechanical energy storage applications. *J. Mater. Chem. A* **2019**, *7* (39), 22663−22674.

(11) Lyndon, R.; Konstas, K.; Ladewig, B. P.; Southon, P. D.; Kepert, P. C. J.; Hill, M. R. Dynamic Photo-Switching in Metal−Organic Frameworks as a Route to Low-Energy Carbon Dioxide Capture and Release. *Angew. Chem., Int. Ed.* **2013**, *52* (13), 3695−3698.

(12) Knebel, A.; Geppert, B.; Volgmann, K.; Kolokolov, D. I.; Stepanov, A. G.; Twiefel, J.; Heitjans, P.; Volkmer, D.; Caro, J. Defibrillation of soft porous metal-organic frameworks with electric fields. *Science* **2017**, *358* (6361), 347−351.

(13) Elsaidi, S. K.; Mohamed, M. H.; Banerjee, D.; Thallapally, P. K. Flexibility in Metal−Organic Frameworks: A fundamental understanding. *Coord. Chem. Rev.* **2018**, *358*, 125−152.

(14) Loiseau, T.; Serre, C.; Huguenard, C.; Fink, G.; Taulelle, F.; Henry, M.; Bataille, T.; Férey, G. A Rationale for the Large Breathing of the Porous Aluminum Terephthalate (MIL-53) Upon Hydration. *Chem. - Eur. J.* **2004**, *10* (6), 1373−1382.

(15) Carrington, E. J.; McAnally, C. A.; Fletcher, A. J.; Thompson, S. P.; Warren, M.; Brammer, L. Solvent-switchable continuous-breathing behaviour in a diamondoid metal−organic framework and its influence on CO_2 versus CH_4 selectivity. *Nat. Chem.* **2017**, *9* (9), 882−889.

(16) Lee, J. H.; Jeoung, S.; Chung, Y. G.; Moon, H. R. Elucidation of flexible metal-organic frameworks: Research progresses and recent developments. *Coord. Chem. Rev.* **2019**, *389*, 161−188.

(17) Yang, Q.-Y.; Lama, P.; Sen, S.; Lusi, M.; Chen, K.-J.; Gao, W.-Y.; Shivanna, M.; Pham, T.; Hosono, N.; Kusaka, S.; Perry Iv, J. J.; Ma, S.; Space, B.; Barbour, L. J.; Kitagawa, S.; Zaworotko, M. J. Reversible Switching between Highly Porous and Nonporous Phases of an Interpenetrated Diamondoid Coordination Network That Exhibits Gate-Opening at Methane Storage Pressures. *Angew. Chem., Int. Ed.* **2018**, *57* (20), 5684−5689.

(18) Abylgazina, L.; Senkovska, I.; Ehrling, S.; Bon, V.; St Petkov, P.; Evans, J. D.; Krylova, S.; Krylov, A.; Kaskel, S. Tailoring adsorption induced switchability of a pillared layer MOF by crystal size engineering. *CrystEngComm* **2021**, *23* (3), 538−549.

(19) Ryder, M. R.; Civalleri, B.; Bennett, T. D.; Henke, S.; Rudić, S.; Cinque, G.; Fernandez-Alonso, F.; Tan, J.-C. Identifying the Role of Terahertz Vibrations in Metal-Organic Frameworks: From Gate-Opening Phenomenon to Shear-Driven Structural Destabilization. *Phys. Rev. Lett.* **2014**, *113* (21), No. 215502.

(20) Park, S. H.; Peralta, R. A.; Moon, D.; Jeong, N. C. Dynamic weak coordination bonding of chlorocarbons enhances the catalytic performance of a metal−organic framework material. *J. Mater. Chem. A* **2022**, *10* (44), 23499−23508.

(21) Peralta, R. A.; Huxley, M. T.; Lyu, P.; Díaz-Ramírez, M. L.; Park, S. H.; Obeso, J. L.; Leyva, C.; Heo, C. Y.; Jang, S.; Kwak, J. H.; Maurin, G.; Ibarra, I. A.; Jeong, N. C. Engineering Catalysis within a

Saturated In(III)-Based MOF Possessing Dynamic Ligand−Metal Bonding. *ACS Appl. Mater. Interfaces* **2023**, *15* (1), 1410−1417.
(22) Dutta, A.; Pan, Y.; Liu, J.-Q.; Kumar, A. Multicomponent isoreticular metal-organic frameworks: Principles, current status and challenges. *Coord. Chem. Rev.* **2021**, *445*, No. 214074.
(23) Feng, L.; Wang, K.-Y.; Day, G. S.; Ryder, M. R.; Zhou, H.-C. Destruction of Metal−Organic Frameworks: Positive and Negative Aspects of Stability and Lability. *Chem. Rev.* **2020**, *120* (23), 13087−13133.
(24) Gong, W.; Chen, Z.; Dong, J.; Liu, Y.; Cui, Y. Chiral Metal−Organic Frameworks. *Chem. Rev.* **2022**, *122* (9), 9078−9144.
(25) Khan, U.; Nairan, A.; Gao, J.; Zhang, Q. Current Progress in 2D Metal−Organic Frameworks for Electrocatalysis. *Small Struct.* **2023**, *4* (6), No. 2200109.
(26) Lawson, H. D.; Walton, S. P.; Chan, C. Metal−Organic Frameworks for Drug Delivery: A Design Perspective. *ACS Appl. Mater. Interfaces* **2021**, *13* (6), 7004−7020.
(27) Xie, L. S.; Skorupskii, G.; Dincă, M. Electrically Conductive Metal−Organic Frameworks. *Chem. Rev.* **2020**, *120* (16), 8536−8580.
(28) Zhang, S.; Wang, J.; Zhang, Y.; Ma, J.; Huang, L.; Yu, S.; Chen, L.; Song, G.; Qiu, M.; Wang, X. Applications of water-stable metal-organic frameworks in the removal of water pollutants: A review. *Environ. Pollut.* **2021**, *291*, No. 118076.
(29) Yuan, S.; Zou, L.; Li, H.; Chen, Y.-P.; Qin, J.; Zhang, Q.; Lu, W.; Hall, M. B.; Zhou, H.-C. Flexible Zirconium Metal-Organic Frameworks as Bioinspired Switchable Catalysts. *Angew. Chem., Int. Ed.* **2016**, *55* (36), 10776−10780.
(30) Haldar, R.; Matsuda, R.; Kitagawa, S.; George, S. J.; Maji, T. K. Amine-Responsive Adaptable Nanospaces: Fluorescent Porous Coordination Polymer for Molecular Recognition. *Angew. Chem., Int. Ed.* **2014**, *53* (44), 11772−11777.
(31) Horcajada, P.; Serre, C.; Maurin, G.; Ramsahye, N. A.; Balas, F.; Vallet-Regí, M.; Sebban, M.; Taulelle, F.; Férey, G. Flexible Porous Metal-Organic Frameworks for a Controlled Drug Delivery. *J. Am. Chem. Soc.* **2008**, *130* (21), 6774−6780.
(32) Su, Y.; Otake, K.-I.; Zheng, J.-J.; Horike, S.; Kitagawa, S.; Gu, C. Separating water isotopologues using diffusion-regulatory porous materials. *Nature* **2022**, *611* (7935), 289−294.
(33) Yang, F.; Xu, G.; Dou, Y.; Wang, B.; Zhang, H.; Wu, H.; Zhou, W.; Li, J.-R.; Chen, B. A flexible metal−organic framework with a high density of sulfonic acid sites for proton conduction. *Nat. Energy* **2017**, *2* (11), 877−883.
(34) Mason, J. A.; Oktawiec, J.; Taylor, M. K.; Hudson, M. R.; Rodriguez, J.; Bachman, J. E.; Gonzalez, M. I.; Cervellino, A.; Guagliardi, A.; Brown, C. M.; Llewellyn, P. L.; Masciocchi, N.; Long, J. R. Methane storage in flexible metal−organic frameworks with intrinsic thermal management. *Nature* **2015**, *527* (7578), 357−361.
(35) Sławek, A.; Roztocki, K.; Majda, D.; Jaskaniec, S.; Vlugt, T. J. H.; Makowski, W. Adsorption of n-alkanes in ZIF-8: Influence of crystal size and framework dynamics. *Microporous Mesoporous Mater.* **2021**, *312*, No. 110730.
(36) Taylor, M. K.; Runčevski, T.; Oktawiec, J.; Bachman, J. E.; Siegelman, R. L.; Jiang, H.; Mason, J. A.; Tarver, J. D.; Long, J. R. Near-Perfect CO2/CH4 Selectivity Achieved through Reversible Guest Templating in the Flexible Metal−Organic Framework Co(bdp). *J. Am. Chem. Soc.* **2018**, *140* (32), 10324−10331.
(37) Koupepidou, K.; Nikolayenko, V. I.; Sensharma, D.; Bezrukov, A. A.; Vandichel, M.; Nikkhah, S. J.; Castell, D. C.; Oyekan, K. A.; Kumar, N.; Subanbekova, A.; Vandenberghe, W. G.; Tan, K.; Barbour, L. J.; Zaworotko, M. J. One Atom Can Make All the Difference: Gas-Induced Phase Transformations in Bisimidazole-Linked Diamondoid Coordination Networks. *J. Am. Chem. Soc.* **2023**, *145* (18), 10197−10207.
(38) Roztocki, K.; Sobczak, S.; Smaruj, A.; Walczak, A.; Gołdyn, M.; Bon, V.; Kaskel, S.; Stefankiewicz, A. R. Tuning the guest-induced spatiotemporal response of isostructural dynamic frameworks towards efficient gas separation and storage. *J. Mater. Chem. A* **2023**, *11*, 18646−18650, DOI: 10.1039/D3TA02167J.
(39) Roztocki, K.; Formalik, F.; Bon, V.; Krawczuk, A.; Goszczycki, P.; Kuchta, B.; Kaskel, S.; Matoga, D. Tuning Adsorption-Induced Responsiveness of a Flexible Metal−Organic Framework JUK-8 by Linker Halogenation. *Chem. Mater.* **2022**, *34* (7), 3430−3439.
(40) Ehrling, S.; Miura, H.; Senkovska, I.; Kaskel, S. From Macro- to Nanoscale: Finite Size Effects on Metal−Organic Framework Switchability. *Trends Chem.* **2021**, *3* (4), 291−304.
(41) Sakata, Y.; Furukawa, S.; Kondo, M.; Hirai, K.; Horike, N.; Takashima, Y.; Uehara, H.; Louvain, N.; Meilikhov, M.; Tsuruoka, T.; Isoda, S.; Kosaka, W.; Sakata, O.; Kitagawa, S. Shape-Memory Nanopores Induced in Coordination Frameworks by Crystal Downsizing. *Science* **2013**, *339* (6116), 193−196.
(42) Krause, S.; Reuter, F. S.; Ehrling, S.; Bon, V.; Senkovska, I.; Kaskel, S.; Brunner, E. Impact of Defects and Crystal Size on Negative Gas Adsorption in DUT-49 Analyzed by In Situ 129Xe NMR Spectroscopy. *Chem. Mater.* **2020**, *32* (11), 4641−4650.
(43) Cerasale, D. J.; Ward, D. C.; Easun, T. L. MOFs in the time domain. *Nat. Rev. Chem.* **2022**, *6* (1), 9−30.
(44) Senkovska, I.; Bon, V.; Abylgazina, L.; Mendt, M.; Berger, J.; Kieslich, G.; Petkov, P.; Luiz Fiorio, J.; Joswig, J.-O.; Heine, T.; Schaper, L.; Bachetzky, C.; Schmid, R.; Fischer, R. A.; Pöppl, A.; Brunner, E.; Kaskel, S. Understanding MOF Flexibility: An Analysis Focused on Pillared Layer MOFs as a Model System. *Angew. Chem., Int. Ed.* **2023**, *62* (33), No. e202218076.
(45) Yang, Q.; Wiersum, A. D.; Llewellyn, P. L.; Guillerm, V.; Serre, C.; Maurin, G. Functionalizing porous zirconium terephthalate UiO-66(Zr) for natural gas upgrading: a computational exploration. *Chem. Commun.* **2011**, *47* (34), 9603−9605.
(46) Zlotea, C.; Phanon, D.; Mazaj, M.; Heurtaux, D.; Guillerm, V.; Serre, C.; Horcajada, P.; Devic, T.; Magnier, E.; Cuevas, F.; Férey, G.; Llewellyn, P. L.; Latroche, M. Effect of NH2 and CF3 functionalization on the hydrogen sorption properties of MOFs. *Dalton Trans.* **2011**, *40* (18), 4879−4881.
(47) Giménez-Marqués, M.; Galve, N. C.; Palomino, M.; Valencia, S.; Rey, F.; Sastre, G.; Vitórica-Yrezábal, I. J.; Jiménez-Ruiz, M.; Rodríguez-Velamazán, J. A.; González, M. A.; Jordá, J. L.; Coronado, E.; Espallargas, G. M. Gas confinement in compartmentalized coordination polymers for highly selective sorption. *Chem. Sci.* **2017**, *8* (4), 3109−3120, DOI: 10.1039/C6SC05122G.
(48) Thommes, M.; Kaneko, K.; Neimark, A. V.; Olivier, J. P.; Rodriguez-Reinoso, F.; Rouquerol, J.; Sing, K. S. W. Physisorption of gases, with special reference to the evaluation of surface area and pore size distribution (IUPAC Technical Report). *Chem. Int.* **2015**, *87* (9−10), 1051−1069, DOI: 10.1515/ci-2016-0119.
(49) Kim, Y. K.; Hyun, S.-M.; Lee, J. H.; Kim, T. K.; Moon, D.; Moon, H. R. Crystal-Size Effects on Carbon Dioxide Capture of a Covalently Alkylamine-Tethered Metal-Organic Framework Constructed by a One-Step Self-Assembly. *Sci. Rep.* **2016**, *6* (1), No. 19337.